ISSN 1063-7761, Journal of Experimental and Theoretical Physics, 2015, Vol. 120, No. 5, pp. 886–893. © Pleiades Publishing, Inc., 2015.
Original Russian Text © S.A. Lyashchenko, Z.I. Popov, S.N. Varnakov, E.A. Popov, M.S. Molokeev, I.A. Yakovlev, A.A. Kuzubov, S.G. Ovchinnikov, T.S. Shamirzaev, A.V. Latyshev, A.A. Saranin, 2015, published in Zhurnal Eksperimental'noi i Teoreticheskoi Fiziki, 2015, Vol. 147, No. 5, pp. 1023–1031.

ELECTRONIC PROPERTIES OF SOLID

Analysis of Optical and Magnetooptical Spectra of Fe_5Si_3 and Fe_3Si Magnetic Silicides Using Spectral Magnetoellipsometry

S. A. Lyashchenko[a,b], Z. I. Popov[a,b], S. N. Varnakov[a,b], E. A. Popov[a], M. S. Molokeev[b,f], I. A. Yakovlev[a,b], A. A. Kuzubov[b,c], S. G. Ovchinnikov[a,b,c], T. S. Shamirzaev[d], A. V. Latyshev[d], and A. A. Saranin[e]

[a] *Reshetnikov Siberian State Aerospace University, Krasnoyarsk, 660014 Russia*
[b] *Kirensky Institute of Physics, Siberian Branch, Russian Academy of Sciences, Krasnoyarsk, 660036 Russia*
[c] *Siberian Federal University, Krasnoyarsk, 660041 Russia*
[d] *Rzhanov Institute of Semiconductor Physics, Siberian Branch, Russian Academy of Sciences, Novosibirsk, 630090 Russia*
[e] *Institute for Automation and Control Processes, Far East Branch, Russian Academy of Sciences, Vladivostok, 690041 Russia*
[f] *Far Eastern State Transport University, Khabarovsk, 680021 Russia*
e-mail: lsa@iph.krasn.ru

Received October 27, 2014

Abstract—The optical, magnetooptical, and magnetic properties of polycrystalline ($Fe_5Si_3/SiO_2/Si(100)$) and epitaxial $Fe_3Si/Si(111)$ films are investigated by spectral magnetoellipsometry. The dispersion of the complex refractive index of Fe_5Si_3 is measured using multiangle spectral ellipsometry in the range of 250–1000 nm. The dispersion of complex Voigt magnetooptical parameters Q is determined for Fe_5Si_3 and Fe_3Si in the range of 1.6–4.9 eV. The spectral dependence of magnetic circular dichroism for both silicides has revealed a series of resonance peaks. The energies of the detected peaks correspond to interband electron transitions for spin-polarized densities of electron states (DOS) calculated from first principles for bulk Fe_5Si_3 and Fe_3Si crystals.

DOI: 10.1134/S1063776115050155

1. INTRODUCTION

It is well known that ferromagnet/semiconductor multilayer structures can be used for designing a spin transistor in which the value of the spin current can be varied by controlling the magnetization states of ferromagnetic layers, thus producing a current valve. The usually high spin injection factor in such devices is manifested when a sharp interface separates the ferromagnet from the semiconductor [1], which is technologically difficult to obtain. The traditional solution to the problem of creating a sharp interface is the epitaxial growth of thin ferromagnetic films on the semiconductor. In spintronics devices, silicon is successfully used as the semiconducting layer in view of its weak spin–orbit interaction, long relaxation period, and the leading role of silicon technologies in contemporary microelectronics [2]. For the ferromagnetic layer, 3*d* metals (in particular, iron) are traditionally used [3]. A large number of publications are devoted to investigating the transport, structural, and magnetic properties of Fe/Si systems, including ferromagnetic silicides Fe_5Si_3 and Fe_3Si in iron.

Silicide Fe_3Si is characterized by a large electron spin polarization factor [4, 5] and can be grown epitaxially on a Si(111) single crystal [6, 7]. In turn, the Fe_5Si_3 silicide implanted in silicon demonstrates the giant magnetoresistance effect (2400%) [1], but is thermodynamically unstable in the bulk state at room temperature [8].

The electronic structure of Fe_5Si_3 and Fe_3Si silicide films, which determines their optical and magnetooptical properties, has not been studied comprehensively as yet. The electronic structure and the spectral optical properties of Fe_3Si have been studied in detail in only two publications [6, 9]. However, the spectral magnetooptical properties of Fe_5Si_3 and Fe_3Si have not been analyzed in the literature except for measurement of Faraday rotation in a Fe_5Si_3 polycrystalline film [10].

The electronic and magnetic properties are usually analyzed using optical spectroscopy, SQUID magnetometry, and nuclear magnetic resonance. Such a complex of measurements can take a lot of time and is inconvenient for analyzing thin-film samples with developed surfaces or with a small amount of ferromagnetic material. We will show that the measurement of the spectral dispersion of the permittivity tensor by spectral ellipsometry combined with the magnetooptical Kerr effect makes it possible to obtain information on the electronic properties of the ferromagnet/semiconductor structure in a single measuring cycle.

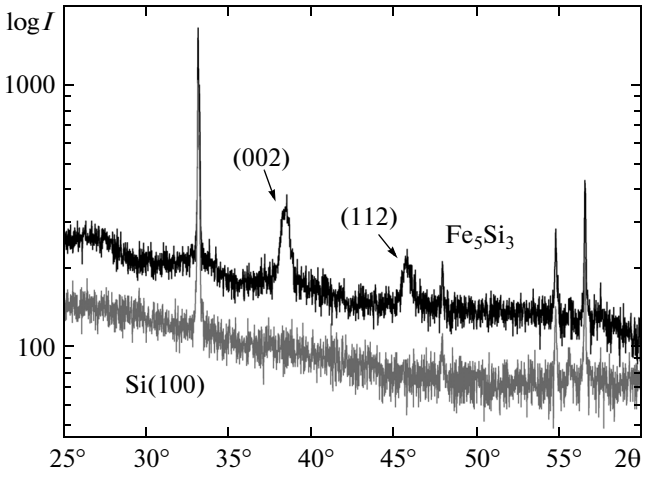

Fig. 1. X-ray diffraction pattern for $Fe_5Si_3/SiO_2/Si(100)$ sample.

2. EXPERIMENTAL

The Fe_3Si epitaxial film was obtained by coprecipitation of Fe and Si in ultrahigh vacuum on a Si(111) 7×7 surface in a modernized Angara molecular beam epitaxy setup [11]. The method for preparing the substrate and obtaining the given structure is described in detail in [7]. According to the spectral ellipsometry data, the total thickness of the Fe_3Si layer was 27 nm. The results of determining the spectral dependence of the complex refractive index N for Fe_3Si from multiangle spectral ellipsometry data are also given in [6].

The polycrystalline Fe_5Si_3 film was also grown using a modernized Angara molecular-beam epitaxy setup [11] by alternate deposition of subnanometer Fe and Si layers on the $SiO_2/Si(100)$ surface at a substrate temperature of 50°C in ultrahigh vacuum. The SiO_2 layer with a thickness of about 13.6 nm was formed by thermal oxidation of the Si(100) substrate in an O_2 + HCl medium at a temperature of 1000°C. After oxidation, the substrate was degreased according to the method proposed in [7], placed in an ultrahigh vacuum, and then annealed at 250°C.

Alternate precipitation of 36 Fe and Si layers was carried out by thermal evaporation from Knudsen effusion cells. The thickness of each Fe and Si layer was 0.5–0.8 nm. The total thickness of the Fe–Si structure was about 27 nm when recalculated to the density of bulk pure materials or 10.7 ± 0.6 μg/cm^2 for Fe and 3.1 ± 0.1 μg/cm^2 for Si. After deposition, the sample was annealed in ultrahigh vacuum at 450°C for 30 min. To identify the crystalline structure of the resultant layer, X-ray diffraction analysis on the sample was carried out on a D8 ADVANCE powder diffractometer ($CuK_{\alpha 1,2}$-radiation, Ni filter) with a VANTEC linear detector, which revealed the presence of the Fe_5Si_3 phase (Fig. 1). The presence of other crystalline phases has not been detected either because of their insignificant volume fraction as compared to Fe_5Si_3 or their highly disperse state with a crystallite size smaller than 2–3 nm. The Fe_5Si_3 polycrystalline film has predominant orientations of crystallites on the (002) and (112) planes.

Analysis of the electronic structure of a ferromagnet from the magnetooptical measurement data requires information about all elements of the permittivity tensor ε of the material. In the case of an optically isotropic ferromagnet (with a small gyromagnetic contribution), the diagonal components of tensor ε are determined from the complex refractive index $N = n + ik$ of the material in the demagnetized state ($N^2 = \varepsilon_m$), while the nondiagonal components of ε are characterized by the Voigt complex magnetooptical parameter $Q = Q_1 + iQ_2$:

$$\varepsilon = \begin{bmatrix} \varepsilon_m & -i\varepsilon_m Q & 0 \\ i\varepsilon_m Q & \varepsilon_m & 0 \\ 0 & 0 & \varepsilon_m \end{bmatrix}. \quad (1)$$

When an external magnetic field is acting on a ferromagnetic material, the polarization properties of ions of this material change relative to the right- or left-circularly polarized external electromagnetic wave, which in turn leads to different refractive indices for the two linear polarization states of light passing through the sample.

The imaginary component of the complex Faraday effect, or magnetic circular dichroism (MCD), which is convenient for analyzing spin-polarized interband transitions of electrons, is given by

$$\psi_F = \frac{\pi}{\lambda}\mathrm{Im}(NQ), \quad (2)$$

where λ is the wavelength of incident radiation [12, 13].

The spectral dependence of complex magnetooptical parameter Q was measured in our experiments on an Ellipse-1891 high-speed spectral ellipsometer with application of an external magnetic field to the sample. In the experimental setup, we used the measuring scheme for the equatorial Kerr magnetooptical effect [14], in which the quantity being measured is the relative variation in the intensity of linearly polarized light reflected from the sample after its passage through the analyzer of the ellipsometer [15]:

$$\frac{\delta I}{I}(t_1, t_2) = 2\frac{I_\uparrow - I_\downarrow}{I_\uparrow + I_\downarrow}, \quad (3)$$

where $I_\uparrow$ and $I_\downarrow$ are the intensities of radiation incident on the photodetector upon magnetization reversal in the sample, and t_1 and t_2 are the angles of rotation of the polarizer and the analyzer of the ellipsometer relative to the plane of incidence of light. Quantity $\delta I/I$

characterizes variation in the reflectance of the surface of the ferromagnet upon its magnetization reversal.

An algorithm for calculating Q from the results of spectral measurements of the value of $\delta I/I$ for various positions of the polarizer and analyzer was proposed in [16]. This algorithm was developed for the model of a semi-infinite ferromagnetic medium or for an absorbing film in the case when light reflected from lower-lying layers does not reach the photodetector. In the case of reflection from the lower nonmagnetic layers, the contribution from the Faraday effect, which changes the resultant calculated Voigt parameter Q predominantly in the low-energy spectral region, occurs in magnetooptical signal $\delta I/I$ apart from the Kerr effect. This contribution affects the amplitude of Q. The main peaks in the MCD are not displaced on the energy scale, but only change their shape the more strongly, the lower the energy values at which they are detected.

According to [16], the value of Q was calculated by the formula

$$\begin{aligned} Q = i\left(B_1 - i\frac{B_2 - B_1B_6}{\sqrt{B_5 - B_6^2}}\right) \\ \times [\sin(2\varphi_0) - \sin(2\varphi_1)]\sin(\varphi_0 + \varphi_1) \\ \times \cos(\varphi_1)\{\cos(\beta)\sin(2\varphi_0)\sin^2(\varphi_1)\}^{-1}, \end{aligned} \tag{4}$$

where φ_0 and φ_1 are the angles of incidence and refraction of light, β is the angle formed by the magnetization of the sample with the plane of incidence of light, and B_{1-6} are real-valued coefficients that can be determined by measuring $\delta I/I$. The magnetization angle β is defined as

$$\beta = \Re\left\{\arctan\left(-\frac{(B_4 - B_3B_6 + iB_3\sqrt{B_5 - B_6^2})\cos(\varphi_0 - \varphi_1)}{2\cos(\varphi_1)(B_2 - B_1B_6 + iB_1\sqrt{B_5 - B_6^2})}\right)\right\}. \tag{5}$$

To calculate the values of n and k for the ferromagnet from the Snell law of refraction, the authors of [16] propose that only coefficients B_5 and B_6 be used:

$$\varphi_1 = -i\ln\left\{\left(\frac{-e^{2i\varphi_0}(1 + B_5 + 2B_6\cos(2\varphi_0) + 2\sqrt{B_5 - B_6^2}\sin(2\varphi_0))}{1 + 2B_6e^{2i\varphi_0} + B_5e^{4i\varphi_0}}\right)^{1/2}\right\}. \tag{6}$$

However, the algorithm proposed in [16] encounters difficulties associated with simultaneous exact calculation by the least square method of all six intermediate coefficients B_{1-6} appearing in the expression for $\delta I/I$. The values of $\delta I/I$ determined by formula (3) appear in the expression

$$\frac{\delta I}{I} = 4\frac{B_1g_1 + B_2g_2 + B_3g_3 + B_4g_4}{B_5g_5 + 2B_6g_4 + g_3}, \tag{7}$$

where $g_i = g_i(t_1, t_2)$ are functions depending on the angles of rotation of the polarized (t_1) and analyzer (t_2). The difficulties associated with simultaneous calculation of all coefficients B_{1-6} are due to large errors in measuring $\delta I/I$ in the case of prolonged accumulation of the useful signal.

To calculate coefficients B_{1-6} exactly and to substantially reduce the time of magnetooptical measurements, we independently calculated coefficients B_5 and B_6 using expression (6), where n and k were determined using multiangle ellipsometry. Using the resulting values of B_5 and B_6 and the system of equations based on expression (7), we calculated coefficients B_{1-4}. Then we calculated complex parameter Q from the values of B_{1-6} for each wavelength. In the search for coefficients B_{1-6}, we used the Nelder–Mead simplex-optimization method [17]. The sweep over the spectrum was performed to both sides from the point with $\lambda = 555$ nm, at which the peak value of the signal-to-noise ratio was attained.

3. ANALYSIS OF EXPERIMENTAL ERRORS

To reduce the error in measuring $\delta I/I$ by formula (3), each of the intensities $I_\uparrow$ and $I_\downarrow$ were measured at least 10 times, after which mean values $\langle I_\uparrow\rangle$ and $\langle I_\downarrow\rangle$ were calculated and standard deviations $\Delta I_\uparrow$ and $\Delta I_\downarrow$ were determined from sampling. The mean value of the resultant magnetic signal was evaluated using formula (3):

$$\left\langle\frac{\delta I}{I}\right\rangle = 2\frac{\langle I_\uparrow\rangle - \langle I_\downarrow\rangle}{\langle I_\uparrow\rangle + \langle I_\downarrow\rangle}, \tag{8}$$

the absolute error in it was determined as the error of indirect reproducible measurements (error propagation law) [18]:

$$\Delta_{\left\langle\frac{\delta I}{I}\right\rangle} = \frac{4\sqrt{(\Delta I_\uparrow\langle I_\downarrow\rangle)^2 + (\Delta I_\downarrow\langle I_\uparrow\rangle)^2}}{(\langle I_\uparrow\rangle + \langle I_\downarrow\rangle)^2}. \tag{9}$$

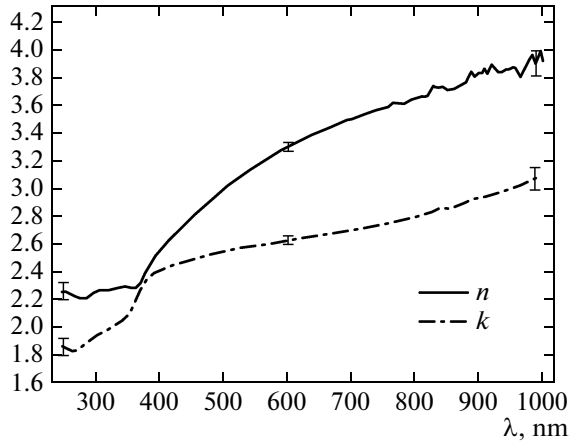

Fig. 2. Measured dispersion of complex refractive index for Fe_5Si_3.

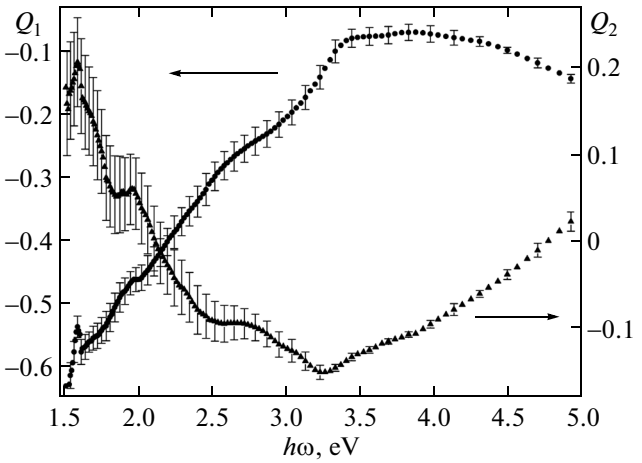

Fig. 3. Calculated dispersion of parameter Q for Fe_5Si_3.

The deviations ΔB_5 and ΔB_6 were determined by numerically calculating the partial derivatives of the difference between expression (6) and the formula for φ_1 from the Snell refraction law with respect to errors Δn, Δk, and $\Delta\varphi_0$. The Nelder–Mead simplex optimization method [17] was used for numerical differentiation of coefficients B_5 and B_6 as well as for determination of their mean values.

The greatest methodical difficulties were associated with estimating errors ΔB_{1-4}, because coefficients B_{1-4} themselves were estimated by solving the system of equations by the least square method. To solve this problem, it is convenient to express each of coefficients B_{1-4} from relation (7) as a function of remaining coefficients B, the measured value of $\langle \delta I/I \rangle$, and the angles of rotation t_1 and t_2 of the optical elements of the ellipsometer. The functions for B_{1-4} obtained in this way were differentiated with respect to each argument. The rms value of ΔB_{1-4} was obtained for each measured $\langle \delta I/I \rangle$ by calculating the error of indirect measurements. The ultimate absolute error for all coefficients B_{1-4} was determined as a result of consistent estimation of ΔB_i for all four values of $\langle \delta I/I \rangle$ and geometrical summation.

The error in magnetooptical parameter Q was calculated by the search method for indirect measurement errors using numerical differentiation of function (4) with respect to each of its arguments. The final search for the error in the MCD value was also carried out using the error propagation law:

$$\Delta\psi_F = \frac{\pi}{\lambda}\mathrm{Im}\left(\sqrt{(\Delta NQ)^2 + (\Delta QN)^2}\right), \qquad (10)$$

where $\Delta N = \Delta n + i\Delta k$ and $\Delta Q = \Delta Q_1 + i\Delta Q_2$ are the corresponding errors for the refractive index of the ferromagnet and its magnetooptical Voigt parameter.

Table 1. Standard deviations S for Fe_5Si_3

Number of peaks	2	3	4	5	6	7
S	0.0490	0.0416	0.0308	0.0250	0.0239	0.0235

4. RESULTS AND DISCUSSION

1. The experimental dependence of the complex refraction index N for Fe_5Si_3 was calculated from the multiangle spectral ellipsometry data [19]. Figure 2 shows the values of n and k of the Fe_5Si_3 film determined using the method described in [19] from multiangle ellipsometric data in the wavelength range of 250–1000 nm.

The value N was calculated from ellipsometric data for polycrystalline Fe_5Si_3 using an optical model of a homogeneous isotropic layer of unknown thickness on the surface of the SiO_2 layer (13.6 nm) with an isotropic Si substrate. The spectral dependences of N for SiO_2 and Si were borrowed from [20, 21].

Parameters $\delta I/I$ were measured ex situ on the $Fe_5Si_3/SiO_2/Si(100)$ sample at room temperature using a spectral magnetoellipsometer for two positions of its analyzer at angles 0° and 45° to the plane of light incidence. The polarizer of the ellipsometer was fixed in position at 45°. A Wollaston prism with two photodetectors as the analyzer allowed us to obtain four independent values of $\delta I/I$ in two cycles of spectral measurements for the following combinations (t_1, t_2): (45°, 0°), (45°, 90°), (45°, 45°), and (45°, 135°). The angle of incidence of light relative to the normal to the sample surface was 70°. The magnetic field in the sample was switched in the range of ±2 kOe. Figure 3

shows the spectral dependences of the real and imaginary parts of the magnetooptical Voigt parameter Q for Fe_5Si_3, calculated from the measured values of $\delta I/I$ and N.

To substantiate the choice of the number m of fitting parameters in the MCD spectrum, we performed calculations with various numbers of Gaussians. Table 1 contains the values of standard deviation

$$S = \sqrt{\frac{1}{n}\sum_{j=1}^{n}\left(\frac{\langle y_j\rangle - f(x_j)}{\langle y_j\rangle}\right)^2}$$

as a function of number m of Gaussian curves in the approximation of the MCD spectrum for Fe_5Si_3, where n is the number of experimental points and $\langle y_j\rangle$ and f_j are the experimental value of the MCD and the sum of all Gaussian curves at point j. The value of S was calculated only for the spectral range of experimental data, which corresponds to the region of fitting by the sum of Gaussian curves. When there are fewer than five peaks, the addition of each next Gaussian sharply reduces deviation S. It can be seen from Table 1 that with increasing number m of Gaussian peaks, the value of S decreases. If, however, the experimental dependence is approximated by five or more peaks, subsequent variation of S is insignificant. Figure 4a shows the energy dependence of MCD calculated by formula (2) with the expansion of the curve into a series of five Gaussians. Individual Gaussian peaks are shown by thin solid curves, while their sum is depicted by the bold solid curve; averaged experimental data are shown by dots. It can be seen that the sum of the Gaussians with given MCDs coincide to within the experimental error.

The energies of probable interband transitions are shown by vertical segments.

To clarify the nature of the detected magnetooptical peaks using quantum-chemical simulation with the VASP 5.3 program package [22–24] based on the density functional technique (DFT) with the basis of plane waves and PAW formalism [25, 26], we performed the spin-polarized calculation of partial densities of electron states (DOS) for Fe_5Si_3 (Fig. 4b). Computations were carried out using the generalized gradient approximation (GGA) of the exchange-correlation Perdew–Burke–Ernzerhof (PBE) functional. In optimizing the geometry of the unit cell $P6_3/mcm$ of Fe_5Si_3, the first Brillouin zone of the reciprocal space was automatically split into a $6 \times 6 \times 6$ grid chosen in accordance with the Monkhorst–Pack scheme [27]. The cutoff energy E_{cutoff} for plane waves in our calculations was 293 eV. In simulating the structure under investigation, geometry optimization was carried out to the value of maximal forces acting on atoms (0.01 eV/A).

The structure of Fe_5Si_3 silicide is characterized by the existence of two nonequivalent states of Fe atoms in the crystal lattice. Analysis of probable interband transitions over the DOS in the energy states of iron

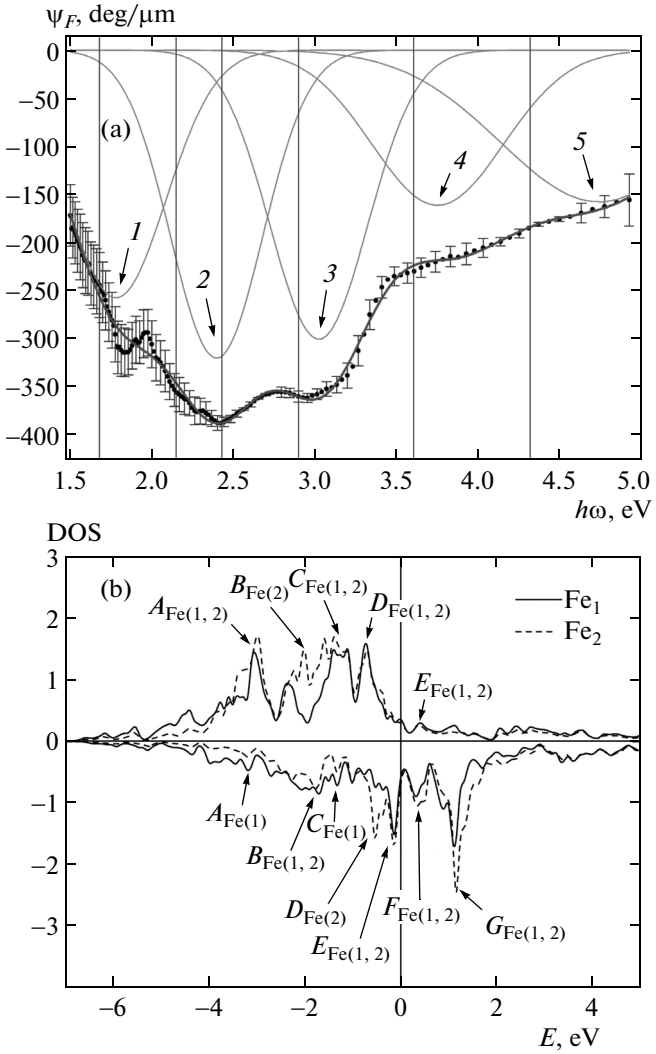

Fig. 4. (a) MCD spectrum for Fe_5Si_3 with expansion into a series of Gaussian curves with following half-width values: (*1*) 1.78 ± 0.36 eV; (*2*) 2.40 ± 0.33 eV; (*3*) 3.02 ± 0.35 eV; (*4*) 3.75 ± 0.47 eV, and (*5*) 4.74 ± 0.71 eV. Vertical lines show the probable interband transitions of electrons by DOS. (b) Theoretical calculation of electron density of states for Fe_5Si_3.

atoms for Fe_5Si_3 shows that the peaks on the Faraday ellipticity curve are due to the following transitions: (*1*) $D_{Fe(2)}\downarrow \longrightarrow G_{Fe(2)}\downarrow$ (1.68 eV); (*2*) $B_{Fe(1,2)}\downarrow \longrightarrow F_{Fe(1,2)}\downarrow$ (2.15 eV) and $B_{Fe(2)}\uparrow \longrightarrow E_{Fe(2)}\uparrow$ (2.42 eV); (*3*) $B_{Fe(1,2)}\downarrow \longrightarrow G_{Fe(1,2)}\downarrow$ (2.9 eV); and (*4*) $A_{Fe(1)}\downarrow \longrightarrow F_{Fe(1)}\downarrow$ (3.6 eV). Peak *5* is in all probability due to the sum of transitions $A_{Fe(1)}\downarrow \longrightarrow G_{Fe(1)}\downarrow$ (4.3 eV) and transitions with a higher energy from the DOS located to the left of $A_{Fe(1)}\downarrow$ to $G_{Fe(1)}\downarrow$.

The best agreement between the peaks detected from MCD and the interband electron transitions is observed in the visible range of the spectrum from 2 to 4.5 eV with the largest signal-to-noise ratio. Our results make it possible to qualitatively determine the origin of the peaks on the MCD spectrum.

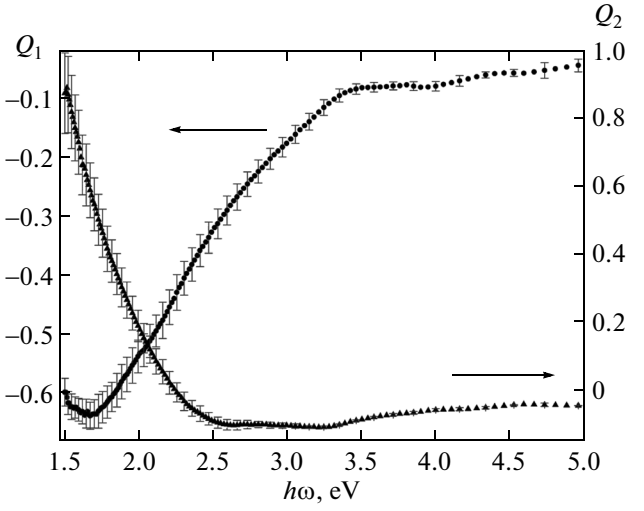

Fig. 5. Calculated dispersion of parameter Q for Fe_3Si.

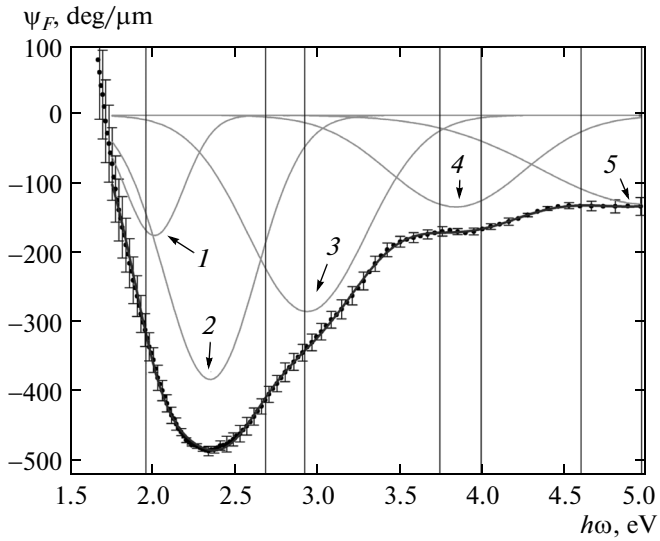

Fig. 6. MCD spectrum for Fe_3Si with expansion into series of Gaussian curves with following half-width values: (*1*) 2.01 ± 0.21 eV; (*2*) 2.35 ± 0.33 eV; (*3*) 2.94 ± 0.42 eV; (*4*) 3.84 ± 0.48 eV, and (*5*) 4.99 ± 0.74 eV. Vertical lines show probable interband transitions of electrons for Fe_3Si according to DOS data from [6].

2. For the $Fe_3Si/Si(111)$ epitaxial structure, we carried out ex situ spectral magnetoellipsometry for parameters $\delta I/I$ at room temperature for two positions of the ellipsometer analyzer at 0° and 45° relative to the plane of incidence of light. The polarizer of the ellipsometer was installed at 45°. The angle of incidence of light formed an angle of 70° with the normal to the sample surface. The magnetic field on the sample was switched on in the range ±2 kOe.

Figure 5 shows the spectral dependences of the real and imaginary parts of magnetooptical Voigt parameter Q for Fe_3Si, calculated from the measured values of $\delta I/I$ and N. Table 2 contains the values of the standard deviation S depending on the number of Gaussian peaks in the MCD approximation for Fe_3Si. It can be seen that with increasing number of Gaussian peaks, the value of S decreases; however, the use of more than five peaks leads to small variations of S as in the case of Fe_5Si_3.

Figure 6 shows the energy dependence of Faraday ellipticity calculated by formula (2) with expansion of the curve into a series of Gaussians. Like for the MCD from Fe_5Si_3, individual Gaussian peaks are shown by thin solid curves; their sum is depicted by the bold solid curve, and averaged experimental data are shown by dots.

In accordance with the spin-polarized DOS calculated in [6] for Fe_3Si, the detected peaks are formed by the following probable interband energy transitions of electrons: (*1*) $E_{Fe(2)}\downarrow \longrightarrow I_{Fe(2)}\downarrow$ (1.96 eV); (*3*) $D_{Fe(1,2)}\downarrow \longrightarrow H_{Fe(1,2)}\downarrow$ (2.68 eV) and $D_{Fe(1,2)}\downarrow \longrightarrow I_{Fe(1,2)}\downarrow$ (2.93 eV); (*4*) $B_{F(1,2)}\downarrow \longrightarrow H_{Fe(1,2)}\downarrow$ (3.74 eV) and $B_{F(1,2)}\downarrow \longrightarrow I_{Fe(1,2)}\downarrow$ (3.99 eV); (*5*) $A_{Fe(1,2)}\downarrow \longrightarrow H_{Fe(1,1)}\downarrow$ (4.60 eV) and $A_{Fe(1,2)}\downarrow \longrightarrow I_{Fe(1,2)}\downarrow$ (4.96). Peak *2* is probably the result of electron transitions from the levels, which are not indicated in [6] and located on the left of the DOS peak $B_{Fe(2)}\uparrow$, to $D_{Fe(2)}\uparrow$.

Table 2. Standard deviations S for Fe_3Si

Number of peaks	2	3	4	5	6	7
S	0.2118	0.0982	0.0958	0.0471	0.0457	0.0416

The results obtained for Fe_3Si make it possible to qualitatively explain the origin of the peaks in the MCD spectrum like for the Fe_5Si_3 film. However, the Fe_3Si epitaxial film demonstrates more exact coincidence of the MCD peaks with the energies of interband transitions as compared to the Fe_5Si_3 polycrystalline film, which may be due to the effect of a smaller fraction of surface atoms in Fe_3Si epitaxial silicide on the spin polarization as compared to polycrystalline Fe_5Si_3.

3. Using the capabilities of magnetoellipsometry in analyzing the magnetic parameters of nontransparent structures [14], we measured the dependences of ellipsometric parameter Ψ for $Fe_3Si/Si(111)$ and $Fe_5Si_3/SiO_2/Si(100)$ samples on the external magnetic field applied to the sample in the range ±200 Oe (Fig. 7) at a wavelength of 466 nm (2.66 eV).

The coercive force H_c of the Fe_3Si film was 49 ± 12 Oe, and the saturation field was on the order of 100 Oe. The coercive force measured for Fe_3Si slightly exceeds the values obtained by other authors [7, 28], including those for films on GaAs(001) and Ge(111)

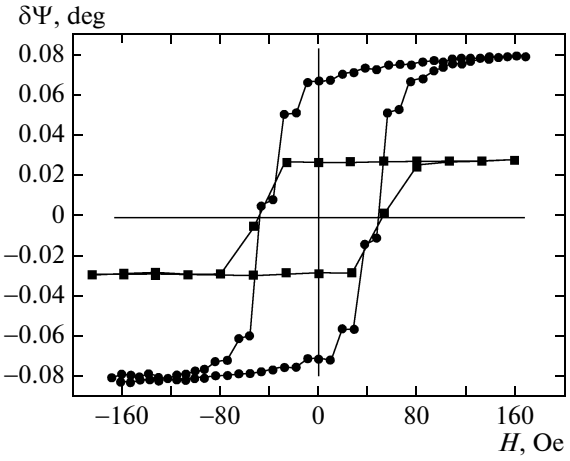

Fig. 7. Magnetization reversal loops for $Fe_3Si/Si(111)$ (■) and $Fe_5Si_3/SiO_2/Si(100)$ (●).

substrates [29, 30]. The coercive force for the Fe_5Si_3 film is close to values measured for Fe_3Si, but it is half as large as the value obtained for the polycrystalline Fe_5Si_3 film with a thickness 65 nm from [10] and slightly exceeds the value of H_c for a Fe_5Si_3 nanofilament at room temperature [31].

5. CONCLUSIONS

We have obtained results of simultaneous analysis of the magnetic, spectral optical, and magnetooptical properties of Fe_5Si_3 and Fe_3Si thin-film silicides using spectral magnetoellipsometry. The application of the algorithm [19] for calculating the optical constants of the structures under investigation made it possible to reduce the experimental time and improve the accuracy of magnetooptical measurements. We have shown that the magnetooptical signals measured for various positions of the analyzer of the ellipsometer can be recalculated into the spectral dependences of the magnetooptical Voigt parameter and magnetic circular dichroism. A series of peaks observed on the spectral dependences of the magnetic circular dichroism in the range 1.6–4.9 eV for Fe_5Si_3 and Fe_3Si silicides correspond to various interband transitions of electrons. Comparison of energies corresponding to the detected resonant peaks on the MCD with the results of ab initio calculations of the electron DOS reveals better agreement between the energies of the peaks and interband transitions of electrons for the Fe_3Si epitaxial film. This is a consequence of the effect of a larger fraction of surface atoms in the polycrystalline film of Fe_5Si_3 silicide on the spin polarization of electrons.

ACKNOWLEDGMENTS

This study was financially supported by the Ministry of Education and Science of the Russian Federation (state assignment no. 16.663.2014K, agreement no. 14.604.21.0002 (RFMEFI60414X0002), and contract no. 02.G25.31.0043), the Program is Support of Leading Scientific Schools (project no. NSh-2886.2014.2), and the Russian Foundation for Basic Research (project nos. 13-02-01265 and 14-02-31309).

REFERENCES

1. P. C. Srivastava and J. K. Tripathi, J. Phys. D: Appl. Phys. **39**, 1465 (2006).
2. I. Appelbaum, B. Huang, and D. J. Monsma, Nature (London) **447**, 295 (2007).
3. A. B. Granovsky, I. V. Bykova, E. A. Gan'shina, V. S. Gushchin, M. Inoue, Yu. E. Kalinin, A. A. Kozlov, and A. N. Yurasov, J. Exp. Theor. Phys. **96** (6), 1104 (2003).
4. H. Haiji, K. Okada, T. Hiratani, M. Abe, and M. Ninomiya, J. Magn. Magn. Mater. **160**, 109 (1996).
5. Y. Maeda, T. Ikeda, T. Ichikawa, T. Nakajima, B. Matsukura, T. Sadoh, and M. Miyao, Phys. Procedia **11**, 200 (2011).
6. I. A. Tarasov, Z. I. Popov, S. N. Varnakov, M. S. Molokeev, A. S. Fedorov, I. A. Yakovlev, D. A. Fedorov, and S. G. Ovchinnikov, JETP Lett. **99** (10), 565 (2014).
7. I. A. Yakovlev, S. N. Varnakov, B. A. Belyaev, S. M. Zharkov, M. S. Molokeev, I. A. Tarasov, and S. G. Ovchinnikov, JETP Lett. **99** (9), 527 (2014).
8. K. S. K. Varadwaj, K. Seo, J. In, P. Mohanty, J. Park, and B. J. Kim, J. Am. Chem. Soc. **129**, 8594 (2007).
9. S. Naderizadeh, S. M. Elahi, M. R. Abolhassani, F. Kanjouri, N. Rahimi, and J. Jalilian, Eur. Phys. J. B **85**, 144 (2012).
10. E. Sawatzky, IEEE Trans. Magn. **7**, 374 (1971).
11. S. N. Varnakov, A. A. Lepeshev, S. G. Ovchinnikov, A. S. Parshin, M. M. Korshunov, and P. Nevoral, Instrum. Exp. Tech. **47** (6), 839 (2004).
12. G. S. Krinchik, *Physics of Magnetic Phenomena* (Moscow State University, Moscow, 1976) [in Russian].
13. E. A. Gan'shina, A. A. Bogoroditskii, R. Yu. Kumaritova, V. V. Bibikova, G. V. Smirnitskaya, and N. I. Tsidaeva, Phys. Solid State **43** (6), 1097 (2001).
14. S. A. Lyashchenko, I. A. Tarasov, S. N. Varnakov, D. V. Shevtsov, V. A. Shvets, V. N. Zabluda, S. G. Ovchinnikov, N. N. Kosyrev, G. V. Bondarenko, and S. V. Rykhlitskii, Tech. Phys. **58** (10), 1529 (2013).
15. G. Neuber, R. Rauer, J. Kunze, J. Backstrom, and M. Rübhausen, Thin Solid Films **455–456**, 39 (2004).
16. R. Rauer, G. Neuber, J. Kunze, J. Bäckström, and M. Rübhausen, Rev. Sci. Instr. **76**, 023910 (2005).
17. J. A. Nelder and R. Mead, Comput. J. **7**, 308 (1965).
18. H. H. Ku, J. Res. Natl. Bur. Stand., Sec. C **70C**, 263 (1966).
19. F. K. Urban III, D. Barton, and T. Tiwald, Thin Solid Films **518**, 1411 (2009).
20. G. Ghosh, Opt. Commun. **163**, 95 (1999).
21. D. E. Aspnes and A. A. Studna, Phys. Rev. B: Condens. Matter **27**, 985 (1983).
22. G. Kresse and J. Hafner, Phys. Rev. B: Condens. Matter **47**, 558 (1993).

23. G. Kresse and J. Hafner, Phys. Rev. B: Condens. Matter **49**, 14251 (1994).

24. G. Kresse and J. Furthmüller, Phys. Rev. B: Condens. Matter **54**, 11169 (1996).

25. P. E. Blöchl, Phys. Rev. B: Condens. Matter **50**, 17953 (1994).

26. G. Kresse and G. D. Joubert, Phys. Rev. B: Condens. Matter **59**, 1758 (1999).

27. H. J. Monkhorst and J. D. Pack, Phys. Rev. B: Solid State **13**, 5188 (1976).

28. K. Hamaya, K. Ueda, Y. Kishi, Y. Ando, T. Sadoh and M. Miyao, Appl. Phys. Lett. **93**, 132117 (2008).

29. A. Ionescu, C. A. F. Vaz, T. Trypiniotis, C. M. Gürtler, H. García-Miquel, J. A. C. Bland, M. E. Vickers, R. M. Dalgliesh, S. Langridge, Y. Bugoslavsky, Y. Miyoshi, L. F. Cohen, and K. R. A. Ziebeck, Phys. Rev. B: Condens. Matter **71**, 094401 (2005).

30. Y. Ando, K. Hamaya, K. Kasahara, K. Ueda, Y. Nozaki, T. Sadoh, Y. Maeda, K. Matsuyama, and M. Miyao, J. Appl. Phys. **105**, 07B102 (2009).

31. K. Seo, S. Lee, Y. Jo, M.-H. Jung, J. Kim, D. G. Churchill, and B. Kim, J. Phys. Chem. C **113** (17), 6902 (2009).

Translated by N. Wadhwa